An empirical many-body potential energy function for modelling ytterbium

1998 J. Phys.: Condens. Matter 10 9419

(http://iopscience.iop.org/0953-8984/10/42/008)

J. Phys.: Condens. Matter **10** (1998) 9419–9429. Printed in the UK PII: S0953-8984(98)93028-4

An empirical many-body potential energy function for modelling ytterbium

Hazel Cox†§, Roy L Johnston‡ and Andrew Ward†

† School of Chemistry, Physics and Environmental Sciences, University of Sussex, Falmer, Brighton BN1 9QJ, UK

‡ School of Chemistry, University of Birmingham, Edgbaston, Birmingham B15 2TT, UK

Received 3 April 1998, in final form 14 August 1998

Abstract. An empirical potential energy function, comprising two- and three-body terms, has been derived for the rare-earth element ytterbium, by fitting parameters to the phonon dispersion curves, elastic constants, lattice energy and lattice distance of the face-centred-cubic (fcc) phase of Yb. This potential reproduces the structural data for fcc Yb, including the negative Cauchy pressure, and correctly accounts for the metastable bcc phase. We predict the bcc phonon dispersion curves (not yet available in the literature) and the activation energy for the Bain transformation between the fcc and bcc phases. The surface energies and relaxations of the high-symmetry surfaces of fcc Yb ((111), (100) and (110)) are calculated for the first time. Furthermore, we predict that the (110) surface of Yb is stable with respect to the 1×2 'missing-row' reconstruction.

1. Introduction

In recent years, an empirical two- plus three-body potential has been developed [1, 2] for simulating the physical properties of metallic elements. The Murrell–Mottram potential has successfully reproduced structural data for a number of metallic solids and has subsequently been used in simulating properties of the bulk, surfaces and clusters [3, 4]. In this model, a number of parameters are fitted to a variety of experimental data, such as the phonon frequencies, the elastic constants and the vacancy formation energy. The two- and three-body components of the potential are simple analytic functions of the interatomic distances.

In contrast with the case for many other potentials, the three-body term is allowed to be either positive or negative, which gives it the advantage of being able to predict a wide range of structures to be the most stable. This is particularly important for Yb, as it can exist as either a hcp, fcc or bcc phase, depending upon the temperature and pressure.

This technique for fitting potentials has been successfully applied to a number of elements, namely: simple metals (Li, Na, K, Ca, Sr, Al) [4–6]; transition metals (Pt, Pd, Fe) [7, 8]; noble metals (Cu, Ag, Au) [9]; semiconductors (C, Si, Ge, Sn) [10]. Confidence in our potential is gained from its applicability to such a wide range of solids. The aim of the present work is to derive a potential capable of reproducing a range of bulk and surface properties of the rare-earth element Yb. This is the first attempt to apply the MM potential to a rare-earth metal, or, indeed, any element with valence f orbitals. Yb is interesting to study as it has two cubic phases (one of which is well documented, but the other less so);

§ Author to whom any correspondence should be addressed.

0953-8984/98/429419+11$19.50

furthermore, it has a negative Cauchy pressure ($C_{12} - C_{44} < 0$) which is a challenge for empirical potentials. Therefore, we hope to use our potential, of proven ability, to predict quantities as yet unknown, such as the bcc phonon dispersion curves. A comparison of this potential with other empirical models in the literature is given elsewhere [11]. In [11] we discuss the analytic form and numerical efficiency, and attempt to give insight into the transferability of our potentials (which are all listed in the appendix of [11]). Our aim is to demonstrate the global applicability of our method.

As mentioned above, Yb is known to undergo two temperature-driven phase transitions at constant pressure [12]. At low temperatures, it has the hcp structure (α-Yb) which undergoes a phase transition at around 260 K to the fcc structure (β-Yb). At 1068 K, just below the melting point, there is another phase transition to the bcc structure (γ-Yb) [13]. Under a pressure of 13 kbar, Yb is thought to undergo a metal-to-semiconductor transformation and at a pressure of 40 kbar the fcc phase undergoes a transformation to the bcc phase. These phase changes have been attributed to pressure-induced broadening of the d bands and their increased hybridization with the s–p bands [14].

The study of the lattice dynamics of Yb has so far been limited, due to the difficulty in producing pure Yb samples, and large single crystals [15]. However, phonon data for the fcc phase of Yb are available [12] as are the elastic constants [16]. Previous theoretical work has primarily been concerned with investigating the dispersion curves of Yb. Ambika Prasad *et al* [17] used a model pseudopotential to interpret the phonon dispersion of both Ca and Yb. They were able to model, with good accuracy, the anisotropic nature of Yb exhibited in the slopes of the T_1 (110) and T_2 (110) branches. More recently, Singh and Singh [18] have used an effective pair potential to calculate the phonon spectra of rare-earth and actinide elemental metals in the fcc phase, along with the binding energy and elastic constants of these metals. Their potential consists of a two-body density-of-states model, and they use second-order perturbation theory for the free-electron part, and a rational dielectric function and the Heine–Abarenkov model for treating the conducting electrons. Band-structure calculations, based on density functional theory, have also been performed, to investigate metal films of Yb grown on metal surfaces [19].

In this paper, we describe the derivation of a Murrell–Mottram potential for Yb by fitting structural and lattice dynamical data for fcc Yb. The potential is also used to predict the (as yet unknown) phonon dispersion curves for metastable bcc Yb, as well as the energies, relaxations and reconstructions of the high-symmetry surfaces of fcc Yb.

2. The model

The Murrell–Mottram potential [1] is based on a many-body expansion of the potential energy V, which is terminated after the three-body term:

$$V = \sum_i \sum_{j>i} V_{ij}^{(2)} + \sum_i \sum_{j>i} \sum_{k>j} V_{ijk}^{(3)} + \cdots . \tag{1}$$

The potential is described in detail elsewhere [1, 4].

The two-body (pair) potential is expressed as

$$V_{ij}^{(2)} = -D(1 + a_2\rho_{ij}) \exp(-a_2\rho_{ij}) \qquad \rho_{ij} = \frac{r_{ij} - r_e}{r_e} \tag{2}$$

and, using the symmetry coordinates Q_i defined as follows:

$$\begin{pmatrix} Q_1 \\ Q_2 \\ Q_3 \end{pmatrix} = \begin{pmatrix} \sqrt{1/3} & \sqrt{1/3} & \sqrt{1/3} \\ 0 & \sqrt{1/2} & -\sqrt{1/2} \\ \sqrt{2/3} & -\sqrt{1/6} & -\sqrt{1/6} \end{pmatrix} \begin{pmatrix} \rho_{ij} \\ \rho_{jk} \\ \rho_{ki} \end{pmatrix} \tag{3}$$

the three-body term has the form

$$V_{ijk}^{(3)} = D\{c_0 + c_1 Q_1 + c_2 Q_1^2 + c_3(Q_2^2 + Q_3^2) + c_4 Q_1^3 + c_5 Q_1(Q_2^2 + Q_3^2) + c_6(Q_3^3 - 3Q_3 Q_2^2)\}F(a_3, Q_1). \tag{4}$$

D and r_e are scaling parameters which ensure that the cohesive energy and the lattice spacing of the reference solid (fcc Yb) are reproduced exactly. The damping function $F(a_3, Q_1)$ makes the three-body term $V_{ijk}^{(3)}$ tend towards zero as Q_1 tends to infinity. Two functions were found to give very good results—sech$(a_3 Q_1)$ and exp$(-a_3 Q_1)$—which both decay exponentially at large values of Q_1 yet have differing short-range behaviour. At short range the exponential damping function can become large and the three-body term can dominate over the two-body term, which may lead to the potential collapsing during the optimization procedure. This is countered by introducing a hard-wall term exp$(-50\{\rho + 0.2\})$, which prevents the nearest-neighbour distance falling below $r_{min} = 0.8r_e$.

Table 1. Data (for fcc Yb) used in the fitting of the MM potential for Yb.

Property				
r_l/Å	5.48			
E_{coh}/eV	1.6			
E_{vac}/eV	0.67			
C_{11}/eV Å^{-3}	0.186			
C_{12}/eV Å^{-3}	0.104			
C_{44}/eV Å^{-3}	0.177			
Mass/g mol^{-1}	173.04			
Frequencies/10^{12} Hz	q	L	T_1	T_2
$[q, 0, 0]$	0.5	0.497	0.377	—
	1.0	1.192	0.708	—
$[q, q, q]$	0.2	0.405	0.082	—
	0.5	1.094	0.278	—
$[q, q, 0]$	0.5	0.828	0.250	0.708
	0.9	0.731	0.693	1.192

3. The potential

The data used in the least-squares fitting of the potential are listed in table 1. The data comprise 14 phonon frequencies taken along the high-symmetry lines $[q00]$, $[qq0]$ and $[qqq]$, three elastic constants and the vacancy formation energy.

Stassis *et al* [12] have measured the phonon dispersion curves for fcc Yb by means of coherent inelastic neutron scattering at room temperature and atmospheric pressure. The large difference in the slopes of the T_1 and T_2 branches in the $[qq0]$ direction implies that fcc Yb is highly anisotropic with respect to the propagation of elastic waves. Data for the bcc and hcp phases are not yet available. In the absence of any direct experimental data

on individual elastic constants, theoretical values obtained by Stassis *et al* [12] were used. They were determined by using a Born–von Kármán harmonic force-constant model to fit the values to the phonon dispersion curves.

A theoretical value for the vacancy formation energy for fcc Yb has been derived from the Debye temperature (measured by means of x-ray powder diffraction at room temperature) by Krishna *et al* [16]. The value of the Debye temperature measured was $\theta_M = 109 \pm 5$ K, which agrees reasonably well with values obtained from calculations based on elastic constants (94 K), the heat capacity (105 K) and the melting point (120 K) [20, 13]. For fcc metals, Glyde [20] has derived a relationship between the Debye temperature and the formation energy of vacancies:

$$E_{vac} = K(k/h)^2 m\theta_M^2 a^2 \tag{5}$$

where k and h are the Boltzmann and Planck constants respectively, a is the interatomic spacing and K is a constant equal to 1.17. A value of 0.67 eV has been calculated for the vacancy formation energy of fcc Yb, which is close to the value of 0.69 eV determined for bcc Yb [16].

In our two-body + three-body model the vacancy energy is given by

$$E_{vac} = -\left[\frac{1}{2}\sum_{j\neq 0} V_{0j}^{(2)} + \frac{2}{3}\sum_{j\neq 0}\sum_{k>j} V_{0jk}^{(3)}\right] \tag{6}$$

where we assume that the relaxation around the vacancy is small; this is usually the case for close-packed metals [5]. The cohesive energy is given by

$$E_{coh} = -\left[\frac{1}{2}\sum_{j\neq 0} V_{0j}^{(2)} + \frac{1}{3}\sum_{j\neq 0}\sum_{k>j} V_{0jk}^{(3)}\right]. \tag{7}$$

4. Results

The search of (a_2, a_3) space revealed a number of potentials which gave a very good fit to the experimental data, correctly predicting the correct energy ordering of the solid structures, with potential energy curves consisting of well-formed single minima which do not collapse at short range. Two potentials were identified as being superior, one involving an exponential damping function ($a_2 = 6$, $a_3 = 8$) and the other involving a hyperbolic secant damping function ($a_2 = 6$, $a_3 = 11$). The coefficients of the two potentials were quite different, reflecting the fact that the exponential and hyperbolic secant potentials differ in how well they reproduce bulk and surface properties. Thus the exp(6, 8) potential gave the best overall fit to the data, whereas the sech(6, 11) potential predicted a first interlayer contraction on the fcc (110) surface, which is consistent with what is known about fcc (110) surfaces of other metals. However, because of the better overall behaviour of the exponential potential, in this paper we report only the results of applying the exp(6, 8) potential. For the optimized MM potential for Yb see table 2.

4.1. Lattice dynamics

Table 3 compares the experimental values of the elastic constants of fcc Yb with those predicted by the MM potential and those obtained by Singh and Singh [18] who quote results obtained using two different dielectric functions. For the purposes of our comparison we took the best result quoted by Singh and Singh in each case. Our calculated elastic constants are within 4% of the experimental values, although the ordering of the C_{11}- and C_{44}-values

Table 2. The optimized MM potential for Yb.

Parameter	Value
a_2	6
a_3	8
F	exp
D/eV	0.300
r_e/Å	4.127
c_0	0.128
c_1	1.306
c_2	2.953
c_3	−1.010
c_4	−0.483
c_5	−2.841
c_6	1.090

Table 3. Bulk properties for fcc Yb, calculated using the MM Yb potential, compared to the experimental values used in the fitting and the *ab initio* calculations of Singh and Singh [18].

Property	Experimental	This work	Reference [18]
E_{vac}/eV	0.67	0.67	—
C_{11}/eV Å^{-3}	0.186	0.181	0.181
C_{12}/eV Å^{-3}	0.104	0.106	0.115
C_{44}/eV Å^{-3}	0.177	0.185	0.175
Anisotropy $= 2C_{44}/(C_{11} - C_{12})$	4.317	4.904	5.303
Bulk modulus $= (C_{11} + 2C_{12})/3$	0.131	0.131	0.137
Compressibility $= 1/$(bulk modulus)	7.614	7.627	7.299
Cauchy pressure $= C_{12} - C_{44}$	−0.073	−0.079	−0.060
Tetragonal shear $= (C_{11} - C_{12})/2$	0.041	0.038	0.033

is wrong due to our overestimating the value of C_{44} and underestimating the value of C_{11}. However, the difference between these two values is very small ($\approx$0.009) and the results that we obtain are closer on average to the experimental values than those obtained by Singh and Singh [18].

For solids in which the atoms lie at centres of inversion symmetry, and in which there are only central interatomic forces (distance-dependent two-body forces), the Cauchy relationship holds ($C_{44} = C_{12}$). There is a 71% difference between these two values for Yb compared with a 15% difference for the alkali metals, showing the importance of many-body forces for Yb. In contrast with the positive values for most metals, the Cauchy pressure ($C_{12} - C_{44}$) for Yb is negative (i.e., $C_{12} < C_{44}$), confirming that many-body forces are necessary to model the bulk properties. Other empirical many-body potentials such as the Sutton–Chen and embedded-atom-method potentials cannot reproduce a negative Cauchy pressure.

The phonon frequencies calculated along the high-symmetry lines in the Brillouin zone are in excellent agreement with the experimental values as shown in figure 1. They are better than the pseudopotential models results of Ambika Prasad *et al* [17] and Singh and Singh [18]. Yb shows a strong anisotropy with regard to elastic waves, as evinced by the difference in slope of the T_1 [$qq0$] and T_2 [$qq0$] branches and the anomalous dispersion of the T_1 [$qq0$] branch between $q = 0.5$ and 0.7, where the frequencies rise above the line for the velocity of sound [12]. Strong similarities can be seen with the dispersion curves of Ca

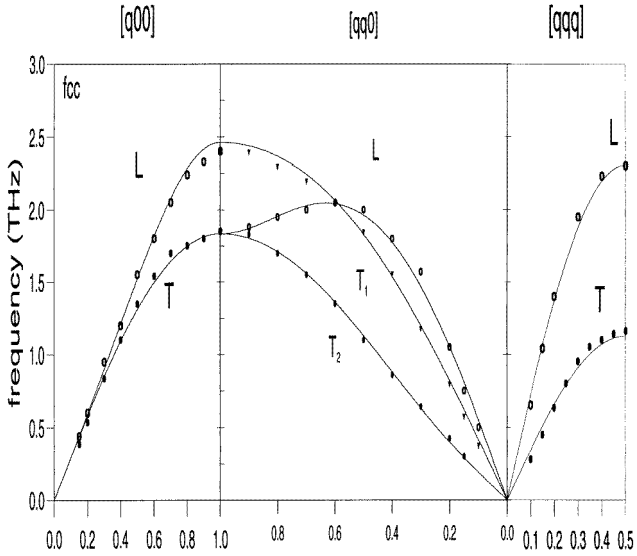

Figure 1. Phonon dispersion curves calculated for fcc Yb. Experimental values are indicated by the points.

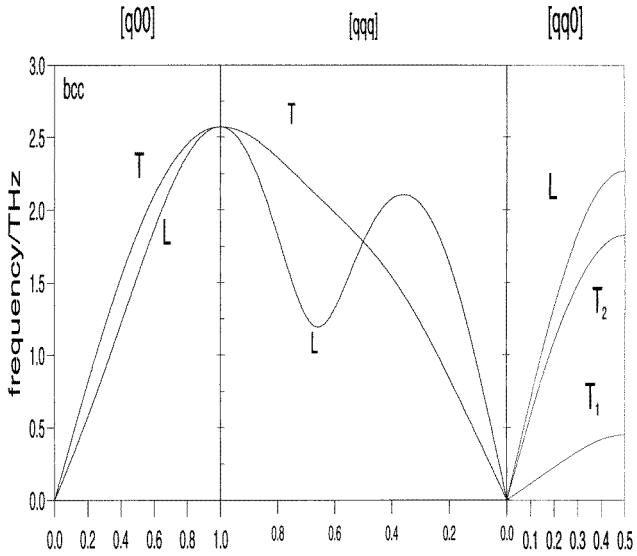

Figure 2. Phonon dispersion curves calculated for bcc Yb.

which have also been successfully modelled with a MM potential [6].

Although the experimental phonon dispersion curves of bcc Yb have not yet been determined, our calculated (predicted) phonon dispersion curves are shown in figure 2. The potential was summed out to eleven shells, in order to obtain a cut-off radius consistent with the fcc calculation. It is interesting to note that the T branch lies above the L branch along the [q00] direction, which is unusual for metals with the bcc structure, but the general shapes of the curves are distinctly bcc-like. All frequencies, throughout the Brillouin zone,

were found to be real—indicating that the bcc structure is a local minimum on the potential energy hypersurface for Yb.

Table 4. Cohesive energies and nearest-neighbour distances calculated for a variety of Yb structures. The values in brackets are experimental distances (from [13] and references therein); see the text for more details.

	Structure	Coordination	E_{coh} /eV	R_{nn}/Å
3D	hcp	12	1.601	3.88 (3.88, 3.90)
	fcc	12	1.600	3.88 (3.88)
	bcc	8	1.595	3.71 (3.84)
	she	8	1.411	3.90
	scu	6	1.286	3.81
	dia	4	0.840	3.81
2D	f111	9	1.219	3.95
	f100	8	1.148	3.92
	f110	6	0.925	3.97
	tri	6	0.861	4.03
	squ	6	0.718	3.97
	hex	3	0.504	4.02

4.2. Structural stabilities

If a potential is to be used to study liquids, surfaces, clusters etc, it is essential that it is shown to be applicable over a wide range of coordination number. The cohesive energies and nearest-neighbour distances have been calculated for a number of two- and three-dimensional structures, as shown in table 4. The 3D structures considered are: hexagonal close packed (hcp), face-centred cubic (fcc), body-centred cubic (bcc), simple hexagonal—AAA stacking of triangular nets (she), simple cubic (scu) and diamond (dia). The 2D structures consist of single layers: triangular net (tri), square net (squ), hexagonal net (hex, i.e. a single graphite layer), and two-layer slabs (f100, f110, f111) corresponding to the top two layers of the fcc (100), (110) and (111) surfaces, respectively. Getting reasonable relative energies for these structures is of great importance if our potential is subsequently to reproduce the properties of surfaces accurately.

In general the stability of a particular structure is found to decrease with decreasing coordination number. We find that the hcp phase is marginally more stable than the fcc phase, which in turn is more stable than the bcc phase. This agrees with the experimental ordering of structures [13]. The values in brackets are the experimental nearest-neighbour distances. For hcp structure, which has two independent lattice constants a and c, the nearest-neighbour distance has been calculated using an idealized hcp structure, in which $c = \sqrt{8/3}\,a$, so all twelve neighbours of an atom in the hcp lattice are at the same distance. The two shortest M–M contacts in hcp metals are: six neighbours at a and six neighbours at $\sqrt{a^2/3 + c^2/4}$. The latter distance reduces to a when c is ideal (i.e., $\sqrt{8/3}\,a$). The experimental values at 296 K are $a = 3.8799$ Å and $c = 6.3859$ Å [21]. Thus the c/a ratio is equal to 1.646 which is close to ideal (1.633) but a little stretched along c. Therefore, using the experimental values, the two nearest-neighbour distances are 3.88 and 3.90 (as quoted in the table); these agree well with our calculated distance of 3.88 for the ideal hcp structure. The shortening of the bcc nearest-neighbour distance, relative to that for the fcc structure, is overestimated.

4.3. The Bain path for fcc–bcc interconversion

There are a large number of possible diffusionless pathways via which one can interchange the fcc and bcc phases [22]. We have studied the tetragonal Bain path. This pathway allows the interconversion to progress with a minimum of atomic movement, and hence strain, in the lattice. The restriction that must be obeyed for this to be valid is that there must be no diffusion and the atoms must be exchangeable. To convert fcc to bcc structure, we contract the lattice parallel to the *c*-axis and expand it parallel to the *a*- and *b*-axes. We have investigated c/a ratios in the range 0.8 to 1.6.

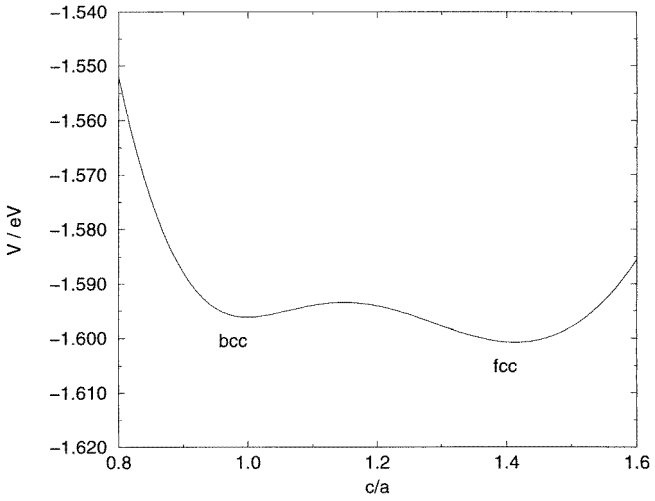

Figure 3. The variation of the potential energy with the c/a ratio for Yb along the tetragonal Bain deformation path.

There are two minima along the Bain path; one corresponds to the fcc structure ($c/a = \sqrt{2}$) and the other corresponds to the bcc structure ($c/a = 1$) (in the bct definition [23]). Figure 3 shows that the fcc structure is lower in energy than the bcc structure, as expected from table 4. To convert the fcc to the bcc structure, we predict an activation energy of 0.0073 eV (0.0027 eV for the reverse transformation).

A contour plot of the potential energy surface (plotted as a function of c/a and the reduced volume V/V_0, where V_0 is the volume per atom of the fcc phase) is shown in figure 4. Only two minima are present on the map, corresponding to the bcc and fcc structures, and the fcc structure is the most stable. This is really quite remarkable considering that no information on the bcc structure was input into the potential fitting procedure.

4.4. Surface energies and relaxations

The interlayer separations at metal surfaces are found to differ from those of the bulk. This is known as surface relaxation and it is common for the outer-layer spacing of the fcc (110) surface to decrease. Structural changes known as reconstructions, which involve movements in the x, y-plane as well as parallel to the z-axis, also occur on some surfaces, as the atoms find a more energetically stable configuration. For fcc structures, the energies of the surfaces decrease in the order of the stability, (111) < (100) < (110), predominantly due to the decreasing coordination of surface atoms on going from the (111) to the (110)

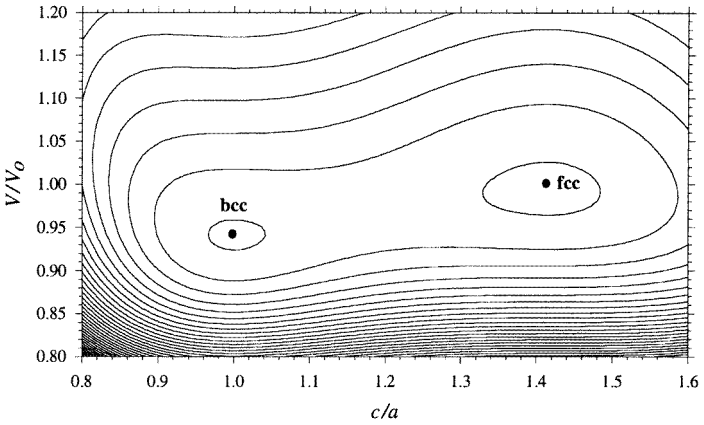

Figure 4. A contour plot of the potential energy surface, for body-centred tetragonal Yb, as a function of c/a and the reduced volume V/V_0. The lowest contour (around the bcc and fcc minima) is that for -1.60 eV and the contour spacing is 0.01 eV.

surface.

Surface relaxations were studied by optimizing the atomic positions in a double-sided slab of atoms having identical surfaces in both the $+z$- and $-z$-directions. These slabs consist of a cuboidal box of: 11 (100) layers with an (x, y) periodicity of 7×7 atoms per layer; 15 (110) layers of 7×6 atoms per layer; and 9 (111) layers of 7×8 atoms per layer. The energy is minimized using the NAG [24] conjugate-gradients routine e04dgf.

The surface energy is calculated as

$$E_s = \frac{NE_{coh} + V}{2A} \tag{8}$$

where V, the total potential energy of the slab, is a negative quantity and E_{coh}, the bulk cohesive energy, is defined as a positive quantity. N is the number of atoms in the slab and A is the surface area.

As far as we are aware, no experimental data exist for the relaxations of these high-symmetry surfaces. However, our surface energies can be compared with the recommended values for the 'average' surface energy at 0 K extrapolated from experimental values [25], the *ab initio* calculations for the (111) surface by Skriver and Rosengaard [26] and the estimated 'average' surface energy from the recent surface tension measurements performed by Bezukladnikova and Kononenko [15] for liquid Yb. Bezukladnikova and Kononenko measured the surface tension using the large-drop method carried out in a high-purity helium atmosphere with a sample containing less than 0.19% impurity. Problems with oxygen retention at the surface gave inaccuracies estimated at 15–20% of the true value by comparison with errors in measurements for other elements. The measurement procedure is still problematic, especially for rare-earth metals, due to oxygen retention, impurities in the metal, difficulties in sample preparation and difficulties in finding the correct choice of experimental parameters.

The solid–vapour free surface energy (γ_{SV}) for an average surface can be derived from the liquid surface tension (γ_{LV}) using the assumption that $\gamma_{SV}/\gamma_{LV} \approx 1.18$ at the melting point, T_m [27]. The γ_{SV}-value is quoted in table 5, along with the experimental value quoted in [25] and the calculated value quoted in [26]. Our calculated (using the bulk-derived potential) values are in good agreement with the 'recommended value' of de Boer

Table 5. Relaxed surface energies E_s (meV Å^{-2}) for the low-index surfaces of fcc Yb.

	(111)	(100)	(110)	$(1 \times 2)^{\dagger}$
This work	29.7	30.4	32.0	33.6
ab initio [26]	24.4			
Experiment [15][a]		26.3		
Experiment [25][b]		31.2		

† The reconstructed (110) surface.
[a] An estimate from the experimental (average) surface tension value.
[b] The recommended experimental surface energy at 0 K.

et al for the 0 K experimental surface energy and the value of $E_s(111)$ calculated by Skriver and Rosengaard who argue that 'the surface energies calculated by present day *ab initio* methods are at least as accurate as the experimental values' [26]. We also predict that the 1×2 reconstructed (110) surface of fcc Yb has a higher surface energy than the unreconstructed surface, which implies that the (110) surface will not reconstruct. It is not currently known, experimentally, whether or not the (110) surface reconstructs.

Table 6. Percentage relaxations calculated for the outer three interlayer spacings of unreconstructed fcc Yb surfaces. Negative values correspond to contractions in interlayer spacings compared to those in the bulk.

Surface	Δd_{12} (%)	Δd_{23} (%)	Δd_{34} (%)
(111)	−0.08	0.06	−0.07
(100)	1.67	0.44	−0.44
(110)	6.22	−1.99	0.84

Our predicted relaxations are listed in table 6. For most metals, there is a contraction of the outer interlayer spacing of the most open fcc (110) surface to compensate for the decrease in coordination. However, our potential predicts an expansion. Given the lack of experimental data, we cannot be sure that our potential is predicting unphysical behaviour or that it possesses too much pair character. There is generally no consensus on the movements of the (111) and (100) metal surfaces except that any movements are small; our results are consistent with this finding.

5. Conclusions

We have derived an empirical two- plus three-body potential energy function for Yb and shown that the MM potential reproduces the experimental structural data of fcc Yb to a high degree of accuracy. The potential also predicts the bcc phase to be metastable. We have presented phonon dispersion curves for bcc Yb and calculated the activation energy required for the fcc–bcc phase change, along the tetragonal Bain path. Furthermore, we have investigated the surface behaviour of fcc Yb. Our calculated surface energies of the high-symmetry surfaces of fcc Yb are in good agreement with the available surface energy data. We have made predictions for the relaxations of these surfaces; on the (111) and (100) surfaces the movements are small, which concurs with the known relaxations in other metals [7, 9]; however, for the open (110) surface we get the surprising prediction of a first interlayer expansion. We have also calculated the energy of the 1×2 reconstructed

(110) surface, which is favoured for some metals (e.g. Au and Pt), but find that for Yb the unreconstructed (110) surface is more stable.

Acknowledgments

HC wishes to thank the Royal Society for the award of a Dorothy Hodgkin Research Fellowship and Dr G A Lawless for suggesting the study of Yb. The authors wish to thank Professor J N Murrell for helpful discussions.

References

[1] Murrell J N and Mottram R E 1990 *Mol. Phys.* **69** 571
[2] Murrell J N 1990 *Phil. Mag.* **69** 571
[3] Andersson K M, Johnston R L and Murrell J N 1994 *Phys. Rev.* B **49** 3089
[4] Cox H, Johnston R L and Murrell J N 1997 *Surf. Sci.* **373** 67
[5] Fang J Y, Johnston R L and Murrell J N 1993 *J. Chem. Soc. Faraday Trans.* **89** 1659
[6] Hearn J E, Johnston R L and Murrell J N 1996 *J. Chem. Soc. Faraday Trans.* **92** 425
[7] Cox H 1998 *Surf. Sci.* **397** 374
[8] Gao F, Johnston R L and Murrell J N 1993 *J. Phys. Chem.* **97** 12 073
[9] Cox H, Liu X and Murrell J N 1998 *Mol. Phys.* **93** 921
[10] Eggen B R, Johnston R L and Murrell J N 1994 *J. Chem. Soc. Faraday Trans.* **90** 3029
[11] Cox H, Johnston R L and Murrell J N 1998 *J. Solid State Chem.* submitted
[12] Stassis C, Loong C K, Theisen C and Nicklow R M 1982 *Phys. Rev.* B **26** 4106
[13] *Handbook on the Physics and Chemistry of Rare Earths* 1978 vol 1, ed K A Gschneidner Jr and L Eyring (Amsterdam: North-Holland)
[14] Johansen G and Mackintosh A R 1970 *Solid State Commun.* **8** 121
[15] Bezukladnikova L L and Kononenko V I 1994 *Izv. Ross. Akad. Nauk Met.* **5** 14
[16] Krishna N G, Sirdeshmukh D B, Rao B R, Beaudry B J and Gschneidner K A Jr 1985 *Phys. Status Solidi* a **89** K37
[17] Ambika Prasad M V N, Gupta H C and Tripathi B B 1984 *Phys. Rev.* B **29** 3708
[18] Singh N and Singh S P 1990 *Phys. Rev.* B **42** 1652
[19] Bodenbach M, Höhr A, Laubschat C, Kaindl G and Methfessel M 1994 *Phys. Rev.* B **50** 14 446
[20] Glyde H R 1967 *J. Phys. Chem. Solids* **28** 2061
[21] Kayser F X 1971 *Phys. Status Solidi* **8** 233
[22] Porter D A and Easterling K E 1981 *Phase Transformations in Metals and Alloys* (New York: Van Nostrand Reinhold)
[23] Bain E C 1924 *Trans. AIME* **70** 25
[24] *The NAG Fortran Library Manual* 1993 16th edn (Oxford: Numerical Algorithms Group Limited)
[25] deBoer F R, Boom R, Mattens W C M, Miedema A R and Niessen A K 1988 *Cohesion in Metals* (Amsterdam: North-Holland)
[26] Skriver H L and Rosengaard N M 1992 *Phys. Rev.* B **46** 7157
[27] Tyson W R and Miller W A 1977 *Surf. Sci.* **62** 267